Available online at www.sciencedirect.com
ScienceDirect
Journal of Sound and Vibration 304 (2007) 246–262
JOURNAL OF SOUND AND VIBRATION
www.elsevier.com/locate/jsvi

Parametric study of dynamics of worm and worm-gear set under suddenly applied rotating angle

M.Y. Chung, D. Shaw*

Department of Power Mechanical Engineering, National Tsing-Hua University, No. 101 Kung Fu Road Section II, Hsin Chu, Taiwan, ROC

Received 13 September 2006; received in revised form 23 January 2007; accepted 25 February 2007
Available online 17 April 2007

Abstract

The dynamics of a worm-gear set under instantly applied rotating angle are affected by several factors (including the friction force and elastic deformation of the surface between gear teeth). It is found that those factors cause a non-negligible rotational positioning error. The goals of this study are to (1) set up a mathematic model, (2) carry out a numerical simulation, and (3) carry out an experiment and compare it with the numerical results. The experiments and numerical results have very good agreement. In this research, the moment-inertia of fly wheel, friction, rigidity of shaft and rigidity of gear tooth are also studied. The results can be used as error estimations of relevant angles, angular speed and angular acceleration under a suddenly applied rotational angle, and are useful for establishing the error compensation required for position control.
© 2007 Elsevier Ltd. All rights reserved.

1. Introduction

When radar tracks an aircraft which turns at a sharp angle; the radar may not be able to lock onto the target due to the small oscillation of the antenna. Sometimes, the oscillation even causes a failure of the radar system. Accurate positioning is a crucial subject in a tracking system. However, due to the design of the tracking transmission mechanism is restricted by both space and weight, the volume and the weight of the transmission mechanism must be limited. The worm-gear set is a good choice due to its small volume and high reduction ratio. Owing to the oscillation of the antenna is an important dynamics behavior for high precision positioning of radar system, the dynamics of a worm-gear set under instantly applied large torque is very important to understand this behavior. This behavior is affected by several factors including the friction force and elastic deformation of the surface between gear teeth. To understand the effect of those factors, a lot of research has been conducted. Yuksel and Kahraman [1] studied the influence of surface wear on the dynamic behavior of a typical planetary gear set. The wear model employed a quasi-static gear contact model to compute contact pressures and Archard's wear model to determine the wear depth distributions. Parker et al. [2] analyzed the dynamic response of a spur pair of a wide range of operating speeds and torques. Comparisons were made to other researchers' published experiments that reveal complex nonlinear phenomena. The dynamic response of

*Corresponding author. Tel.: +88635742604; fax: +88635739979.
E-mail addresses: dishaw@pme.nthu.edu.tw, t0102065@seed.net.tw (D. Shaw).

0022-460X/$ - see front matter © 2007 Elsevier Ltd. All rights reserved.
doi:10.1016/j.jsv.2007.02.022

a spur pair was investigated using a finite element/contact mechanics model that offers significant advantages for dynamic gear analyses. Maliha [3] created a nonlinear dynamic model of a spur gear pair, which was coupled with linear finite element models of the shafts carrying them, and with discrete models of bearings and disks. The excitations considered in the model were external static torque and internal excitation caused by mesh stiffness variation, gear errors and gear tooth profile modification. Britton [4] produced a super finished gear teeth (with a approximately 0.05 μm Ra Film) and the friction traction in the experiments were simulated theoretically using a thin film non-Newtonian micro-elastohydrodynamic lubrication solver and encouraging agreement between friction measurements and theoretical predictions was obtained. Kong [5] predicted elastic contact and elastohydrodynamic film thickness in worm gears. Using the undeformed geometry of the gap between gear teeth in contact a three-dimensional elastic contact simulation technique had been developed for calculation of the true area of elastic contact under load relative the wheel and worm surfaces. Tuttle [6] studied the harmonic drives, which exhibited very nonlinear dynamic behavior, in his model not only dynamic models include accurate representation of transmission friction, compliance and kinematical error were understand, but also important features of harmonic-drive gear-tooth geometry and interaction. Experimental observations were used to guide the development of a model to describe harmonic-drive operation.

It is important to be aware that worm-gear performance is influenced by the lubricant applied and maintained. Helouvry [7] discussed the issue of the servo-orientation control being affected by a surge of both maximum static friction force and dynamic friction force. They reported the occurrence of a stable positioning error, as well as the stopping (or stoking) during tracking at the turning point of a limiting loop of the tracking system. When the system was in a one directional low-speed tracking, it was possible for the stick–slip phenomenon to occur due to the fact that the frictional force to velocity curve appears to be a negative slope and influences the static friction force. It was also found that a similar phenomenon occurs at high-speed tracking. Doupont [8] proposed a frictional force model with negative slope. In the reference, relative motion from static to high-speed sliding was divided into four stages. In the first stage, the external force was less than the maximum static friction force. In the second stage, two contacting surfaces started to develop a small relative velocity. In the third stage, the relative velocity started to increase between two objects, and lubricant got into the contact area and decreased the frictional force. In the fourth stage, the lubricant had fully filled the contact area, and the viscous characteristic and the frictional force increased with the velocity. Oguri design handbook [9] included several empirical charts and calculation formulae of the friction coefficient vs. sliding velocity, the allowable error of manufacturing, the recommended value for the gaps between two teeth, and the allowable contact pressure. Shigley [10] discussed the worm's pitch circle line velocity as well as the transmission frictional coefficient.

In the transmission drives, the deformation of the teeth is effected by the contact load of the teeth surfaces. Simon [11] utilized the finite element method to investigate the effects of the design parameters on the surface stress distribution of the worm-gear tooth. Octure [12] presented a method to calculate the stress distribution on the worm-gear teeth, and derived the material requirements for the worm-gear tooth to sustain the loading. Sudoh et al. [13] employed a laser projection method to study the stress distribution of worm and worm-gear teeth, and compared them with theoretical values. The Japan Gear Manufacturer Association [14] specified the gear tooth basic contact patterns. From these patterns, the precision of the gear set and the loading positions could be analyzed.

In above researches, the dynamic behavior of gear set was exhibited. Bair [15] studied the duel-lead worm that has two different axial modules for its right- and left-side tooth surfaces; the worm thickness was different along its axial cross-section. The backlash of a mating ZK-type duel-lead worm-gear drives can be reduced or eliminated by adjusting the worm axial meshing position. Fang [16] developed the mathematical model of ZK-type worm-gear set that was based on the cutting mechanism and its tool parameters. Variations in bearing contact due to pitch diameter variations of oversize hob cutters and center distance variations of worm[gear set were also investigated Seol [17] developed an approach, which have been applied to K-type of single enveloping worm-gear drives and also developed theory to investigate the influence of misalignment on the shift of the bearing contact, the transmission errors and the contact ratio. The purpose was to reduce the sensitivity of the worm-gear drive to misalignment. William [18] found that in the optimum conditions when two gears of finite diameter mesh and rotated, the contact of any worm-gear tooth profile is line contact. Depending on the flexibility of the gear tooth, a contact area of greater or lesser size is produced by a

corresponding elastic deformation of the tooth surfaces. The coefficient of friction was influenced by the materials, lubricants, Hertzian stresses, sliding conditions along the contact line, tooth forms, diameters, and positions of the relative to the worm. Dual lead worm gears could be run in either direction of rotation and, on such sets, the backlash was adjustable to zero.

In this study, only the friction force and elastic deformation of the surface between gear teeth are interested. The ZK-type worm-gear set is used to eliminate the backlash. Previous research works on gears and gear sets were focused on the limiting loading, pressure distribution and allowable pressure loading of gears, and on the relationship between friction coefficient and sliding velocity. Most investigations are base on the assumption that the tooth is rigid. This study is focused on the effects of the elastic deformation of the gear tooth surface and the nonlinear friction coefficient on the system dynamics. To study the dynamics of the worm-gear set, a dynamic model of the worm-gear set is developed and the comparison between the experimental results and the numerical results is also studied. The parameters of the dynamic model are adjusted by the findings of the comparison of the analysis and the experiment. Finally, the effects of moment-inertia of fly wheel, friction, rigidity of shaft and rigidity of gear tooth on the nonlinear behavior of the transmission mechanism are also studied.

2. The dynamic models of the worm-gear set

2.1. The equilibrium equations of the worm and worm-gear set

The geometric of worm-gear set is shown in Fig. 1. There are a worm, a worm gear, two shafts, four bearings and a flywheel. The shaft of worm is driven by an angle θ_1. The rotational angle of the flywheel is θ_4. The rotational angle of the worm's body is θ_2 (due to the elastic deformation of the worm shaft; $\theta_1 \neq \theta_2$). The rotation angle of worm-gear body is θ_3. The moment of inertia of the worm is J_w. The pitch radius of the worm's helical tooth is r_w. The worm's rotational inertia as a rigid body is J_g. The pitch radius of the worm gear is r_g. The moment-inertia of the flywheel is J_4. In this study, to neglect the effect of backlash, ZK-type worm and worm gear are used both in analysis and experiment.

To simplify the theoretical model, the basic assumptions are listed as follows:

(1) The flywheel is rigid.
(2) The worms and worm-gear teeth are elastic.
(3) The body of the worm gear is rigid.
(4) Worm and worm gear are perpendicular to each other.
(5) The clearance between teeth is ignored.
(6) No error on the gear tooth profile.

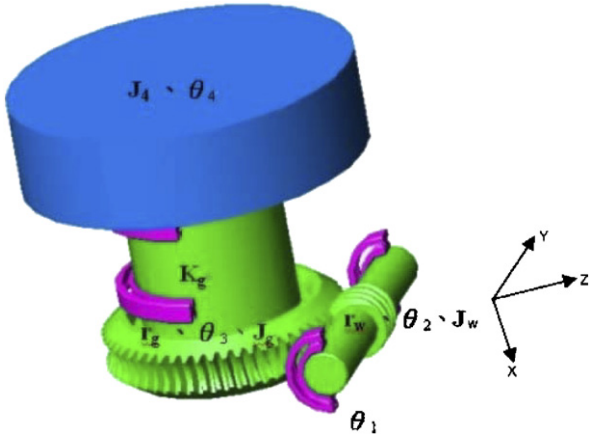

Fig. 1. Geometric of worm and worm gear.

(7) The worm is single thread.
(8) The worm shaft and worm-gear shaft are two rotational spring. The dynamic behavior is neglected.
(9) Translational degree-of-freedom for all the elements is not considered.
(10) Only friction is considered, no other damping effect is considered.

To set up the equilibrium equations of worm and worm-gear set. The normal force W_n and friction force W_f between the teeth of the worm and the teeth of the worm gear are needed to be decomposed and projected into three orthogonal force components F_X, F_Y and F_Z as shown in Fig. 2 and can be expressed as follows:

$$F_X = W_n \cos \phi_n \sin \lambda + W_f \cos \lambda, \tag{1}$$

$$F_Y = W_n \cos \phi_n \cos \lambda - W_f \sin \lambda, \tag{2}$$

$$F_Z = W_n \sin \phi_n. \tag{3}$$

In above equations, ϕ_n is the pressure angle and λ is the worm's lead angle. It is noted that in Eqs. (1)–(3), the normal force W_n and the friction force W_f are the function of the rotating angle and angular velocity of worm and worm gear. In this study, the relation between normal force and friction forces is $W_f = \mu W_n$.

The equilibrium equations of motion can be divided into three free bodies. One is the equilibrium equation of the worm and worm shaft, the other is the equilibrium equation of worm gear and shaft and another is the equilibrium equation of flywheel. The equilibrium equation of the worm and worm shaft can be expressed as follows:

$$\begin{aligned} J_w\ddot{\theta}_2 &= -F_X(\theta_2, \theta_3, \dot{\theta}_2, \dot{\theta}_3) r_w - K_w(\theta_2 - \theta_1) \\ &= -(W_n(\theta_2, \theta_3, \dot{\theta}_2, \dot{\theta}_3) \cos \phi_n \sin \lambda) r_w - (W_f(\theta_2, \theta_3, \dot{\theta}_2, \dot{\theta}_3) \cos \lambda) r_w - K_w(\theta_2 - \theta_1). \end{aligned} \tag{4}$$

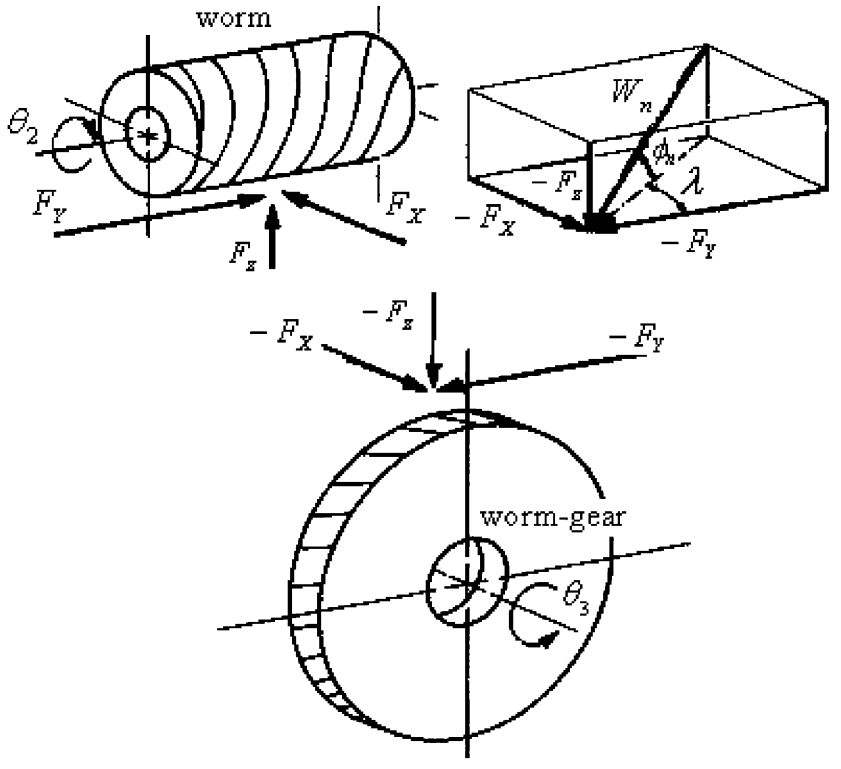

Fig. 2. Contact forces decomposition.

In above equation, K_w is the elastic constant of the worm shaft. The total torque applied on the worm and worm shaft is the force $F_X(\theta_2, \theta_3, \dot{\theta}_2, \dot{\theta}_3)$ applied on the tooth times the pitch circle of the worm. This torque induces the deformation of the worm shaft and angular acceleration of the worm. The equilibrium equation of worm gear and worm-gear shaft can be expressed as

$$\begin{aligned} J_g\ddot{\theta}_3 &= F_Y(\theta_2, \theta_3, \dot{\theta}_2, \dot{\theta}_3)r_g - K_g(\theta_3 - \theta_4) \\ &= (W_n(\theta_2, \theta_3, \dot{\theta}_2, \dot{\theta}_3)\cos\phi_n \cos\lambda)r_g - (W_f(\theta_2, \theta_3, \dot{\theta}_2, \dot{\theta}_3)\sin\lambda)r_g - K_g(\theta_3 - \theta_4). \end{aligned} \tag{5}$$

In above equation, the angular acceleration of worm gear and the torsion of the shaft are caused by the torque $F_Y(\theta_2, \theta_3, \dot{\theta}_2, \dot{\theta}_3)r_g$. The elastic constant of the worm-gear shaft is K_g. The equilibrium equation of the flywheel is

$$J_4\ddot{\theta}_4 = -K_g(\theta_4 - \theta_3). \tag{6}$$

The relation between normal force W_n and the deformation of worm tooth δ_w and the relation between normal force W_n and the deformation of worm-gear tooth δ_g should be found first before expression W_n into the form of θ_2 and θ_3. The relations are listed as follows:

$$\delta_w(\theta_2, \theta_3, \dot{\theta}_2, \dot{\theta}_3) = \frac{W_n(\theta_2, \theta_3, \dot{\theta}_2, \dot{\theta}_3)}{c_w k_w(\theta_2, \theta_3)}$$

and

$$\delta_g(\theta_2, \theta_3, \dot{\theta}_2, \dot{\theta}_3) = \frac{W_n(\theta_2, \theta_3, \dot{\theta}_2, \dot{\theta}_3)}{c_g k_g(\theta_2, \theta_3)}.$$

Using above equation, the total deformation due to the rigidity of worm-gear tooth and worm tooth is

$$\delta_w(\theta_2, \theta_3, \dot{\theta}_2, \dot{\theta}_3) + \delta_g(\theta_2, \theta_3, \dot{\theta}_2, \dot{\theta}_3) = W_n(\theta_2, \theta_3, \dot{\theta}_2, \dot{\theta}_3)\frac{c_g k_g(\theta_2, \theta_3) + c_w k_w(\theta_2, \theta_3)}{c_w k_w(\theta_2, \theta_3) c_g k_g(\theta_2, \theta_3)}. \tag{7}$$

In above equation, $c_g k_g(\theta_2,\theta_3)$ is the spring constant of worm-gear tooth and $c_w k_w(\theta_2,\theta_3)$ is the spring constant of worm's helical tooth. The deformation of tooth is normal to the direction of tooth, which has an angle $(\pi/2-\lambda)$ with the shaft axis. The lead angle is λ. To find the relation between rotation angle and the deformation, one must account on all the components of deformation in Y-direction.

According to Fig. 3, the deformations between worm tooth and worm-gear tooth are related by lead angle. When worm is rotated from 0 to θ_2, theoretically, the tooth of the worm is moved to $l_w\theta_2$. The lead of the worm is l_w. But there are deformations of worm tooth $(\delta_w(\theta_2, \theta_3, \dot{\theta}_2, \dot{\theta}_3))$, the deformation of both worm shaft and the bearing $(\delta_{ws}(\theta_2, \theta_3, \dot{\theta}_2, \dot{\theta}_3))$,which effect the true position of the worm tooth. The effective displacement of worm in Y-axis direction is $l_w\theta_2 - \delta_w(\theta_2, \theta_3, \dot{\theta}_2, \dot{\theta}_3)/\sin(\pi/2-\lambda) - \delta_{ws}(\theta_2, \theta_3, \dot{\theta}_2, \dot{\theta}_3)$. When worm gear is rotate from 0 to θ_3, theoretically, the worm gear is moved to $r_g\theta_3$. But there are also deformations of worm-

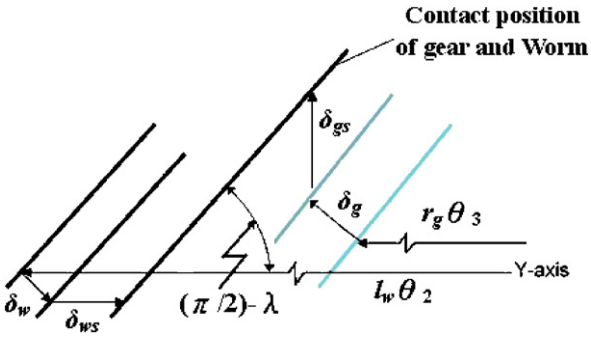

Fig. 3. The deformation of both teeth in Y-axis direction.

gear tooth ($\delta_g(\theta_2,\theta_3,\dot{\theta}_2,\dot{\theta}_3)$) and deformation of worm-gear shaft and the bearing ($\delta_{gs}(\theta_2,\theta_3,\dot{\theta}_2,\dot{\theta}_3)$), which effect the true position of the worm-gear tooth. The effective movement of worm gear in Y-axis direction is $r_g\theta_3+\delta_g(\theta_2,\theta_3,\dot{\theta}_2,\dot{\theta}_3)/\sin(\pi/2-\lambda)+\delta_{gs}(\theta_2,\theta_3,\dot{\theta}_2,\dot{\theta}_3)\cot(\pi/2-\lambda)$. Nevertheless, the continuity at contact position between worm tooth and worm-gear tooth make the movement of worm and worm-gear tooth have the same magnitude. This relation has the following form:

$$r_g\theta_3+\frac{\delta_g(\theta_2,\theta_3,\dot{\theta}_2,\dot{\theta}_3)}{\sin(\pi/2-\lambda)}+\delta_{gs}(\theta_2,\theta_3,\dot{\theta}_2,\dot{\theta}_3)\cot(\pi/2-\lambda)=l_w\theta_2-\frac{\delta_w(\theta_2,\theta_3,\dot{\theta}_2,\dot{\theta}_3)}{\sin(\pi/2-\lambda)}-\delta_{ws}(\theta_2,\theta_3,\dot{\theta}_2,\dot{\theta}_3).$$

Above equation can be rearranged as

$$\frac{(\delta_w(\theta_2,\theta_3,\dot{\theta}_2,\dot{\theta}_3)+\delta_g(\theta_2,\theta_3,\dot{\theta}_2,\dot{\theta}_3))}{\sin(\pi/2-\lambda)}+\delta_{gs}(\theta_2,\theta_3,\dot{\theta}_2,\dot{\theta}_3)\cot(\pi/2-\lambda)+\delta_{ws}(\theta_2,\theta_3,\dot{\theta}_2,\dot{\theta}_3).$$
$$=(l_w\theta_2-r_g\theta_3). \tag{8}$$

In above two equations,

$$\delta_{gs}(\theta_2,\theta_3,\dot{\theta}_2,\dot{\theta}_3)=\frac{F_X(\theta_2,\theta_3,\dot{\theta}_2,\dot{\theta}_3)}{k_{gs}}=\frac{W_n(\theta_2,\theta_3,\dot{\theta}_2,\dot{\theta}_3)(\cos\phi_n\sin\lambda+\mu(\dot{\theta}_2,\dot{\theta}_3)\cos\lambda)}{k_{gs}},$$

$$\delta_{ws}(\theta_2,\theta_3,\dot{\theta}_2,\dot{\theta}_3)=\frac{F_Y(\theta_2,\theta_3,\dot{\theta}_2,\dot{\theta}_3)}{k_{ws}}=\frac{W_n(\theta_2,\theta_3,\dot{\theta}_2,\dot{\theta}_3)(\cos\phi_n\cos\lambda-\mu(\dot{\theta}_2,\dot{\theta}_3)\sin\lambda)}{k_{ws}},$$

where K_{gs} is the axial spring constant of worm-gear shaft and worm-gear bearing and K_{ws} the axial spring constant of worm shaft and worm bearing.

In above equations, the friction coefficient μ is the function of $\dot{\theta}_2$ and $\dot{\theta}_3$, the way to calculate the friction coefficient will be discussed later. Combining (7) and (8), the relation between normal force and rotating angles can be expresses as

$$W_n(\theta_2,\theta_3,\dot{\theta}_2,\dot{\theta}_3)=\frac{(l_w\theta_2-r_g\theta_3)\sin(\pi/2-\lambda)}{KGWS(\theta_2,\theta_3,\dot{\theta}_2,\dot{\theta}_3)}. \tag{9}$$

$$KGWS(\theta_2,\theta_3,\dot{\theta}_2,\dot{\theta}_3)=\frac{c_gk_g(\theta_2,\theta_3)+c_wk_w(\theta_2,\theta_3)}{c_wk_w(\theta_2,\theta_3)c_gk_g(\theta_2,\theta_3)}+\frac{(\cos\phi_n\sin\lambda+\mu(\dot{\theta}_2,\dot{\theta}_3)\cos\lambda)\cos(\pi/2-\lambda)}{k_{gs}},$$
$$+\frac{(\cos\phi_n\cos\lambda-\mu(\dot{\theta}_2,\dot{\theta}_3)\sin\lambda)\sin(\pi/2-\lambda)}{k_{ws}}. \tag{10}$$

Eq. (4) can be expressed as

$$\begin{aligned}J_w\ddot{\theta}_2&=-(W_n(\theta_2,\theta_3,\dot{\theta}_2,\dot{\theta}_3)\cos\phi_n\sin\lambda)r_w-(W_f(\theta_2,\theta_3,\dot{\theta}_2,\dot{\theta}_3)\cos\lambda)r_w-K_w(\theta_2-\theta_1)\\&=-\frac{(l_w\theta_2-r_g\theta_3)\sin(\pi/2-\lambda)}{KGWS(\theta_2,\theta_3,\dot{\theta}_2,\dot{\theta}_3)}r_w(\cos\phi_n\sin\lambda+\mu(\dot{\theta}_2,\dot{\theta}_3)\cos\lambda)-K_w(\theta_2-\theta_1)\\&=-(l_w\theta_2-r_g\theta_3)k_{2wg}(\theta_2,\theta_3,\dot{\theta}_2,\dot{\theta}_3)-K_w(\theta_2-\theta_1),\end{aligned} \tag{11}$$

where

$$k_{2wg}(\theta_2,\theta_3,\dot{\theta}_2,\dot{\theta}_3)=\frac{r_w(\cos\phi_n\sin\lambda+\mu(\dot{\theta}_2,\dot{\theta}_3)\cos\lambda)\sin(\pi/2-\lambda)}{KGWS(\theta_2,\theta_3,\dot{\theta}_2,\dot{\theta}_3)}. \tag{12}$$

Eq. (5) can be rewritten as

$$\begin{aligned} J_g\ddot{\theta}_3 &= F_Y(\theta_2,\theta_3,\dot{\theta}_2,\dot{\theta}_3)r_g - K_g(\theta_3-\theta_4) \\ &= (W_n(\theta_2,\theta_3,\dot{\theta}_2,\dot{\theta}_3)\cos\phi_n\cos\lambda)r_g - (W_f(\theta_2,\theta_3,\dot{\theta}_2,\dot{\theta}_3)\sin\lambda)r_g - K_g(\theta_3-\theta_4) \\ &= W_n(\theta_2,\theta_3,\dot{\theta}_2,\dot{\theta}_3)r_g(\cos\phi_n\cos\lambda - \mu(\dot{\theta}_2,\dot{\theta}_3)\sin\lambda) - K_g(\theta_3-\theta_4) \\ &= \frac{(l_w\theta_2 - r_g\theta_3)\sin(\pi/2-\lambda)}{KGWS(\theta_2,\theta_3,\dot{\theta}_2,\dot{\theta}_3)}r_g(\cos\phi_n\cos\lambda - \mu(\dot{\theta}_2,\dot{\theta}_3)\sin\lambda) - K_g(\theta_3-\theta_4) \\ &= (l_w\theta_2 - r_g\theta_3)k_{3wg}(\theta_2,\theta_3,\dot{\theta}_2,\dot{\theta}_3) - K_g(\theta_3-\theta_4), \end{aligned} \tag{13}$$

where

$$k_{3wg}(\theta_2,\theta_3,\dot{\theta}_2,\dot{\theta}_3) = \frac{r_g(\cos\phi_n\cos\lambda - \mu(\dot{\theta}_2,\dot{\theta}_3)\sin\lambda)\sin(\pi/2-\lambda)}{KGWS(\theta_2,\theta_3,\dot{\theta}_2,\dot{\theta}_3)}. \tag{14}$$

Rewritten Eqs. (4)–(6) into a matrix form, the final form is shown as following:

$$\begin{bmatrix} J_w & 0 & 0 \\ 0 & J_g & 0 \\ 0 & 0 & J_4 \end{bmatrix}\begin{bmatrix} \ddot{\theta}_2 \\ \ddot{\theta}_3 \\ \ddot{\theta}_4 \end{bmatrix} + \begin{bmatrix} l_w k_{2wg}(\theta_2,\theta_3,\dot{\theta}_2,\dot{\theta}_3) + K_w & -r_g k_{2wg}(\theta_2,\theta_3,\dot{\theta}_2,\dot{\theta}_3) & 0 \\ -l_w k_{3wg}(\theta_2,\theta_3,\dot{\theta}_2,\dot{\theta}_3) & r_g k_{3wg}(\theta_2,\theta_3,\dot{\theta}_2,\dot{\theta}_3) + K_g & -K_g \\ 0 & -K_g & K_g \end{bmatrix} \times \begin{bmatrix} \theta_2 \\ \theta_3 \\ \theta_4 \end{bmatrix} = \begin{bmatrix} K_w\theta_1 \\ 0 \\ 0 \end{bmatrix}. \tag{15}$$

Eq. (15) is the dynamic equation of transmission of worm and worm-gear set. To solve the matrix equation, the Newmark-β method is employed to find the numerically result of the dynamic of worm-gear set. Furthermore, the Newton–Raphson method is also introduced to solve the nonlinear terms in the dynamic equations. In the matrix equation (15), furthermore, there are several important constants such as the axial spring constant of bearings, worm shaft, worm-gear shaft and gear teeth, and the friction coefficient of contact-gear teeth. In the following section, the way to find those parameters will be introduced.

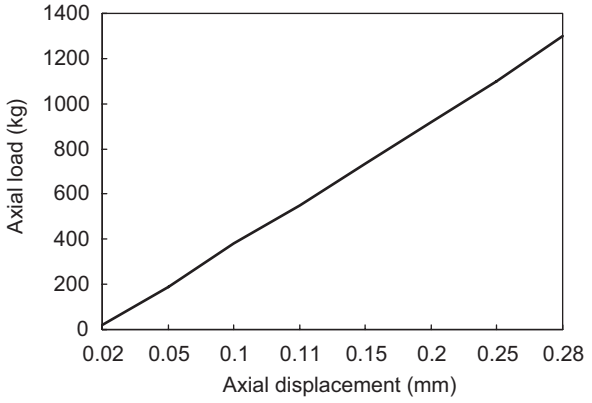

Fig. 4. The relation of axial direction displacements of bearing and axial loads.

2.2. The axial spring constant of bearings, worm shaft and worm-gear shaft

The results of experiment to find the relation between load and the axial displacement of bearing are shown in Fig. 4. The axial spring constant of worm bearing (K_{bTws}) and worm-gear bearing (K_{bTgs}) are obtained by using Fig. 4. Furthermore, K_{Lws} and K_{bTws} can be treat as two series connected spring. As well as K_{Lgs} and K_{bTgs} can also be treat as two series connected spring. Therefore, k_{ws} can be expressed in terms of K_{Lws} with K_{bTws} and k_{gs} can also be expressed in terms of K_{Lgs} with K_{bTgs}. The equations are listed as following:

$$k_{ws} = \frac{K_{Lws}K_{bTws}}{K_{Lws} + K_{bTws}},$$

$$k_{gs} = \frac{K_{Lgs}K_{bTgs}}{K_{Lgs} + K_{bTgs}}.$$

2.3. The spring constant of gear teeth

The solid models of gear teeth were analyzed that the deflection of worm tooth and worm-gear tooth are shown in Fig. 5. The gear body is assumed to be rigid and only the gear tooth is elastic. To simplify the analysis, only 180° of the worm tooth is modeled for analysis because the tooth far away from the loading point does not affect the analysis results. There are different spring constant of worm tooth and worm-gear tooth for different contact positions, the results are shown in Fig. 6. The engineer design the worm and worm-gear system always let gear ratio grater than 1; therefore, there are a lot of chance the worm and worm gear under two teeth contact condition. Considering the contact ratio is 2, the spring constant $c_g k_g(\theta_2,\theta_3)$ and $c_w k_w(\theta_2,\theta_3)$ of the contact tooth can be expresses in the form of Eqs. (16) and (17). Eqs. (16) and (17) are the spring constants of two teeth under different contact position. The curves of $c_g k_g(\theta_2,\theta_3)$ and $c_w k_w(\theta_2,\theta_3)$ are obtained through the method of regression and curve fitting of Fig. 6:

$$\begin{aligned} c_w k_w(\theta_2,\theta_3) &= M e^{aw+bwxwi} + M e^{aw+bwxwj} \\ &= M e^{aw}(e^{bwxwi} + e^{bwxwj}). \end{aligned} \tag{16}$$

In above formula, *xwi* is the contact position (*i*) of worm tooth, *xwj* the contact position (*j*) of worm tooth, *aw* the constant (19.38843319), *bw* the constant (0.000656069) and *M* the modules of worm

$$\begin{aligned} c_g k_g(\theta_2,\theta_3) &= M e^{ag+bgxgi} + M e^{ag+bgxgj} \\ &= M e^{ag}(e^{bgxgi} + e^{bgxgj}). \end{aligned} \tag{17}$$

In above formula, *xgi* is the contact position (*i*) of worm-gear tooth, *xgj* the *j* contact position (*j*) of worm-gear tooth, *ag* the constant (19.64527077), and *bg* the constant (−0.00055956).

2.4. The friction coefficient of contact-gear teeth

The relative motion between worm teeth and worm-gear teeth is considered pure sliding, so the friction plays an important role on the performance of worm-gear set. The efficiency of gear set is directly affected by

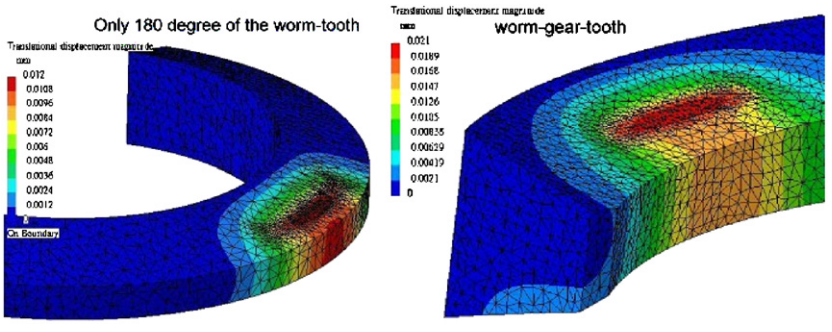

Fig. 5. The FEM model and the deflection of worm tooth and worm-gear tooth under load.

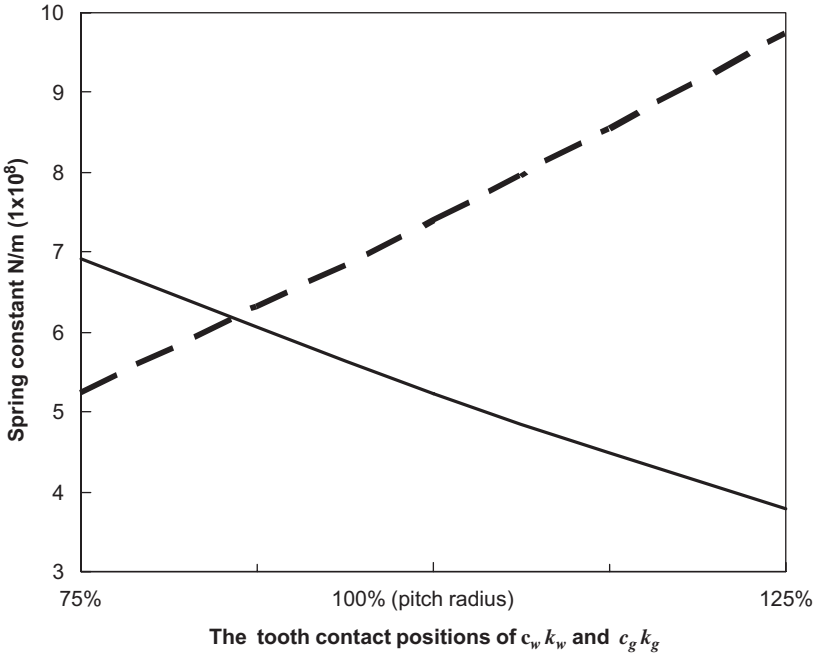

Fig. 6. Spring constant curves of worm teeth and worm-gear teeth for different contact position —— $c_g k_g$, –-- $c_w k_w$.

the coefficient of friction. The coefficient of friction is influenced by the surface sliding speed of the both teeth; the friction is reduced as the relative sliding velocity increases. No formulae can be used to calculate the friction coefficient precisely. In this study, the formula is based on the sliding velocity of the mean worm diameter [8,9,18]:

$$\mu(\dot{\theta}_2, \dot{\theta}_3) = 0.0470713 + 0.1056549e^{-(0.223607v)^{0.5}}. \tag{18}$$

In above formula, v the relative sliding velocity of the mean worm diameter $\left(v = r_w \times \dot{\theta}\right)$, $\dot{\theta}$ the relative Iangular velocity of the mean worm diameter and r_w the pitch radius of the worm's helical tooth.

3. Experimental setup

Experimental setup is shown in Fig. 7 and the specifications of the worm-gear set are listed in Table 1. The ZK-type worm-gear set was used to eliminate the backlash. The reduction ratio of gear set is (1:56) and the module of gear is 2. In Fig. 7, a Compumotor's stepping motor, model no. OEM57-83, (with resolution of 1000 steps/rev [0.36°/step]) was used to drive the worm shaft. An accelerometer (KS77) positioned on the upper location of the worm-gear shaft was used to measure the angle acceleration of θ_2 and θ_4. The angle displacement of θ_2 and θ_4 are obtained by integrated the measured angular acceleration twice. The NI USB-6009 DAQ system equipped with Lab-View software was employed to pick and fetch the voltage data from accelerometer.

At the beginning of the experiment, the system was set at rest condition $(\theta_i, \dot{\theta}_i, \ddot{\theta}_{i,i=2,3,4} = 0)$. The sampling rate of data acquisition was 25×10^{-6} s. When the experiment started, the motor was accelerated to its maximum speed along the worm axis following the required acceleration curve, then stop after the input angle reaches θ_1 ($\theta_1 \cong 0.1130973$ rad, 18 steps). The data-acquisition system recorded the acceleration of the accelerometer which attached on the bar end of worm and gear. The angular acceleration can be calculated from acceleration by using geometric relation.

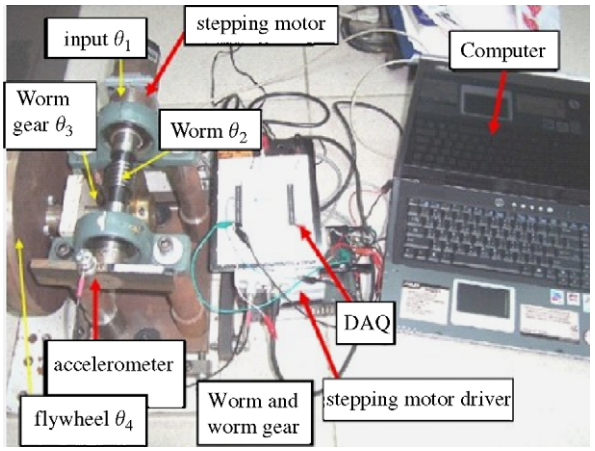

Fig. 7. The experiment device of worm-gear set.

Table 1
Specifications of worm-gear set (modulus M2)

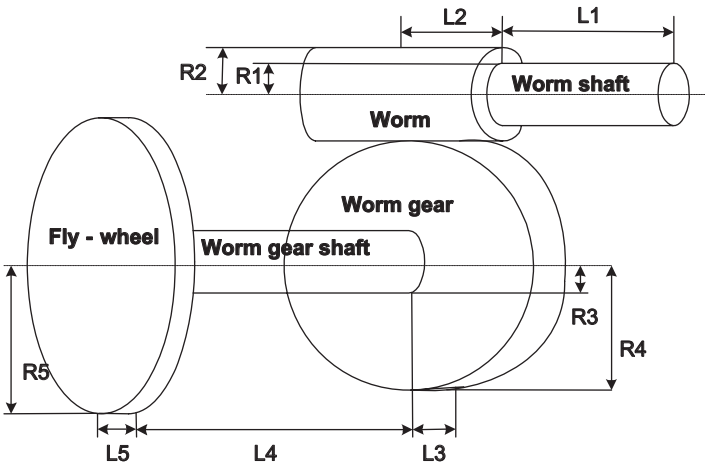

Part	Dimension (m)	Material
Worm shaft	R1 = 0.01534; L1 = 0.20	Steel
Worm	R2 = 0.0158; L2 = 0.015	Chromium molybdenum steel
Worm gear	R3 = 0.056; L3 = 0.02	Phosphorous bronze
Worm gear shaft	R4 = 0.0175; L4 = 0.37	Steel
Fly wheel	R5 = 0.12; L5 = 0.03	Steel
Pressure angle	17°30′	
Lead	0.006283185	
Lead	0.006283185	
Lead angle	3°41′	

3.1. Experimental results

The measurement results of the worm angle acceleration (θ_2 curve) and the flywheel of the worm-gear axis (θ_4 curve) are shown in Fig. 8. The acceleration oscillates between the zero line. The angular acceleration of $\ddot{\theta}_2$ and $\ddot{\theta}_4$ are integrated twice to get angular displacement, which is shown in Fig. 9.

3.2. Comparison between experimental and analytical results

In order to present the oscillation curves of corresponding angles more clearly, the only results of the oscillating part of angular displacement are shown in Figs. 10 and 11. To demo the effect of the nonlinearity, a linear results are also plot in Figs. 10 and 11. For the linear case, the $c_g k_g$ is a constant of 2.5×10^8 N/m, $c_w k_w$ is a constant of 3.5×10^8 N/m and friction coefficient is a constant of 0.145. All parameters of linear case are taken as the mean values of parameters of the nonlinear case. It is found that the frequency of oscillation

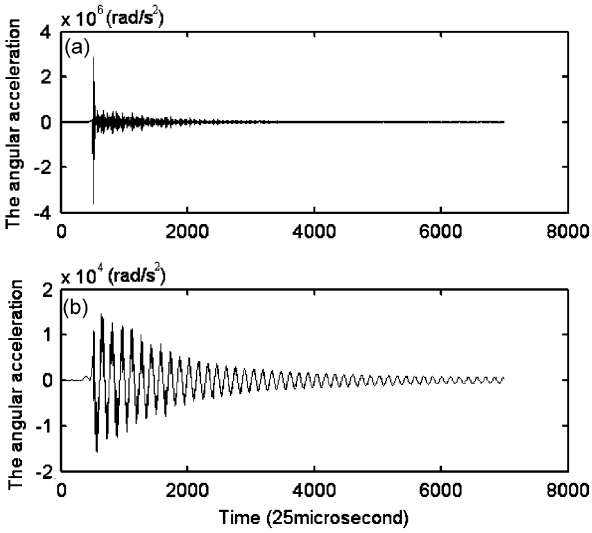

Fig. 8. The measured results: (a) angular acceleration θ_2 and (b) angular acceleration θ_4.

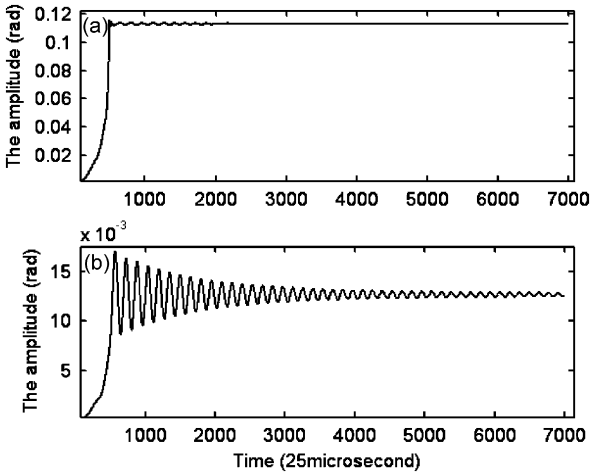

Fig. 9. The angular displacement obtained by integrating the acceleration twice: (a) angle θ_2 and (b) angle θ_4.

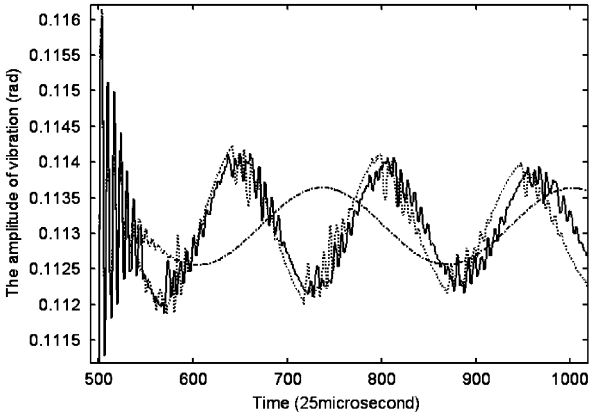

Fig. 10. Comparison of analysis and experiment results of vibration of θ_2 with respect to time (only the overshot part of result are shown) —— simulation, ····· experiment, - - - - linearized.

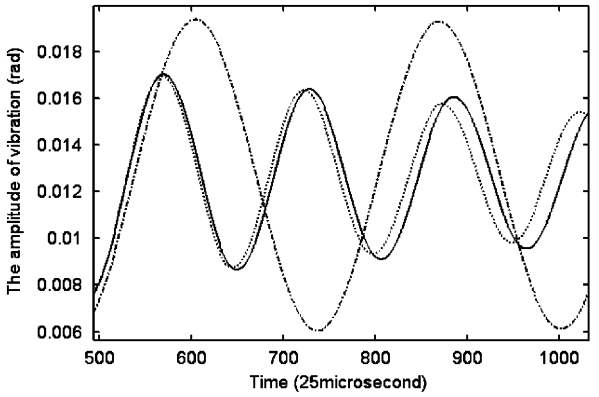

Fig. 11. Comparison of analysis and experiment results of vibration of θ_4 with respect to time (only the overshot part of results are shown) —— simulation, ····· experiment, - - - - linearized.

becomes smaller than the nonlinear case which is due to the nonlinear $c_g k_g$, $c_w k_w$ and friction coefficient make the average of the k_{2wg} and k_{3wg} smaller than the linear one. This results show that the nonlinearity is important for the worm and worm-gear set. For the nonlinear case, the oscillation of θ_2 is between a line of 0.1130973 rad, and The oscillation of θ_4 is between the line of 0.0127076 rad. The maximum difference of the θ_2 between the experimental and analytical results is about 1%. The maximum difference of the θ_4 between the experimental and analytical results is about 1.5% of the mean value.

4. Effect of some parameters

In this study, the worm and worm-gear set is unable to be reversed because the lead angle of worm is small ($\lambda = 3.6^\circ$). At any position of worm suddenly stopped, the worm-gear set is implicated by the flywheel and the kinetic energy of flywheel transmits from flywheel to worm-gear and worm-gear to worm and to worm-shaft bearing. The repeat oscillation of low frequency and large amplitude of the flywheel and worm gear is gradually dissipated by the friction.

The effect parameters will be discussed that included the different diameter of flywheel, the different module of gear, the twist rigidity of worm shaft and worm-gear shaft, the rigidity of the gear tooth and the friction of gear teeth. For more deeply investigation about how transmission system is influenced by these parameters, the module M2 of worm and wore-gear set is analyzed.

The results and discussion are listed as follows.

4.1. The effect of flywheel

To study the effect of the oscillation of the worm-gear set, two cases are studied, one is with flywheel and the other is no-flywheel. As shown in Fig. 12, the thick line is the oscillation of the angles θ_2 and θ_4 with flywheel. The thin line is the oscillation angles without flywheel. It also shown in Fig. 12, the amplitude of the oscillation of θ_2 is smaller than θ_4. The reason is that worm-gear shaft is perpendicular to worm shaft. The kinematics energy of flywheel is very difficult to influence the θ_2 and mainly influences θ_4. It is also noted in Fig. 12, while there is no flywheel attached on worm-gear shaft, the oscillating of worm, worm gear are under high frequency and small amplitude, and the amplitude is decayed faster than the case with flywheel. For more clearly to observe vibration behaviors and the influence of the effect of worm-gear set, two enlarged θ_2 and θ_4 are presented in Fig. 13.

To study the effect of moment-inertia of flywheel more, several different flywheels are analyzed; the results are shown in Fig. 14. One may find when the diameter of the flywheel is reduced gradually, the amplitude of vibration reduced gradually. Due to the lead angle of worm is small; the most energy translates to the worm gear, the deformation of worm shaft and worm-gear tooth. Only a little energy translates to the rotation

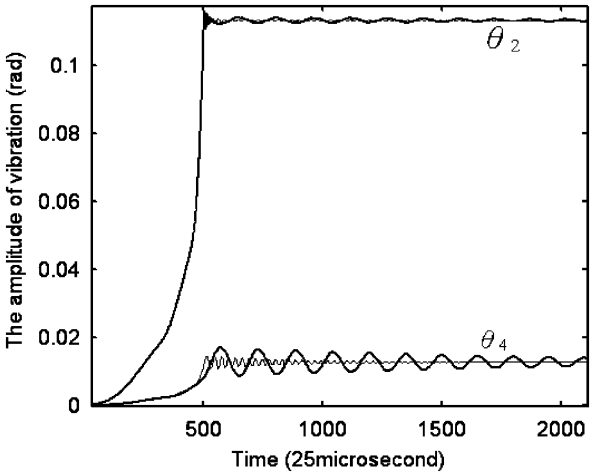

Fig. 12. Effect of moment-inertia of the flywheel on the angular velocity of θ_2 and θ_4.

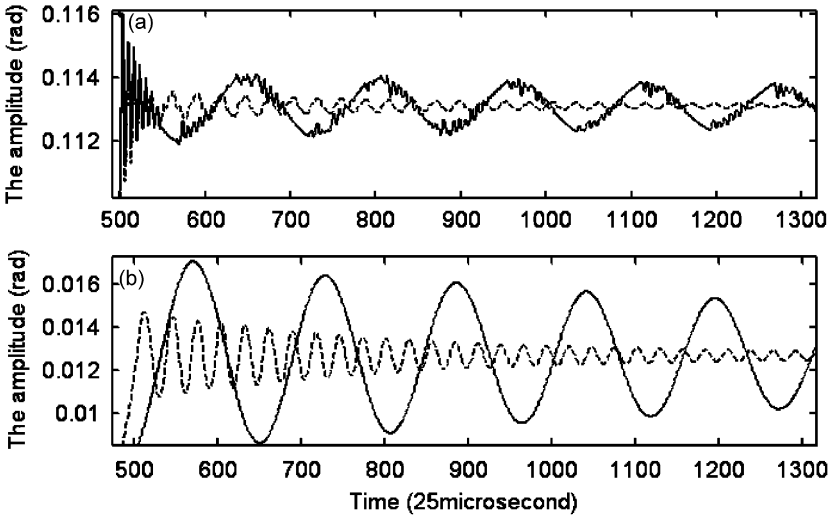

Fig. 13. Effect of moment-inertia of the flywheel on (a) the angular velocity θ_2, – – – without flywheel, —— with flywheel, (b) the angular velocity θ_4, – – – without flywheel, —— with flywheel (only shows the enlarged oscillating part).

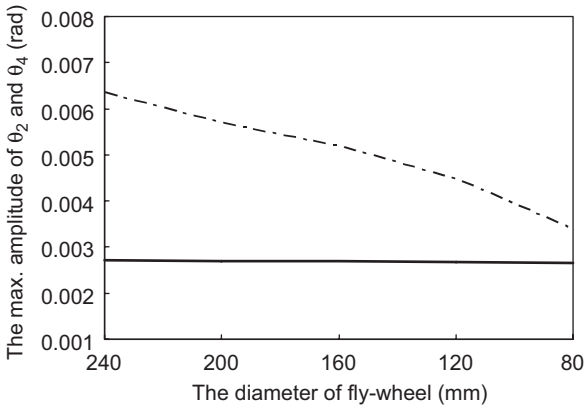

Fig. 14. The result of the flywheel diameter on maximum amplitude of the rotating angles. —— θ_2, – – – θ_4.

direction of worm shaft (θ_2). Because of the effect of moment-inertia of flywheel, the oscillating amplitude of the worm gear is more than the worm.

4.2. The different modulus of gear

As shown in Fig. 15, when the modulus of gear is larger and the rigidity of the teeth is larger. The maximum amplitude of θ_2 and θ_4 are smaller along with the increasing of the gear modulus.

The rotation direction of flywheel is same as the worm gear, but it is perpendicular to the rotational direction of worm. Only a little energy translates to tangential force of worm, which the oscillation–amplitude of worm just changed a little. It is clearly that the reduction of the amplitude of θ_4 is quicker than θ_2 (Mi:the module of gear of i is 1–5).

4.3. The effect of rigidity of worm shaft and worm-gear shaft

To find the effect of the shear modulus of the shaft on the vibration of the gear set, the cases of shear modulus $G(G = 77\,\text{GPa})$ of worm shaft and worm-gear shaft increased gradually until both shafts become

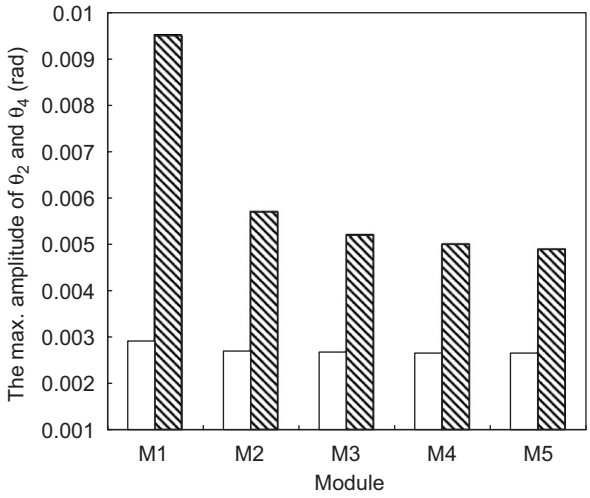

Fig. 15. The maximum oscillating amplitude of θ_2 and θ_4 for M2–M5. □ θ_2, ▨ θ_4.

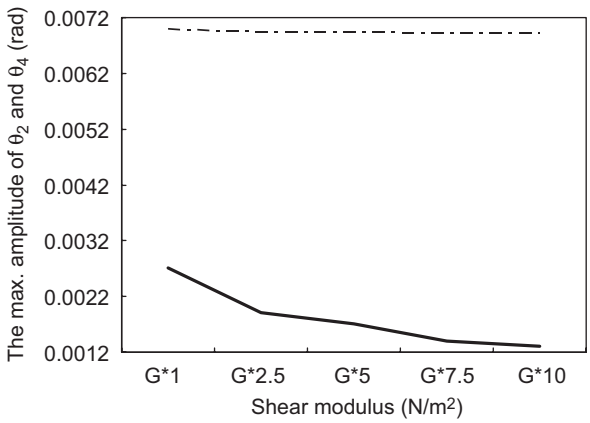

Fig. 16. The effect shear modulus to the maximum oscillating amplitude of worm and worm-gear shafts. —— θ_2, – – – θ_4.

rigid are analyzed. The results are shown in Fig. 16. The θ_2 becomes smaller while the shear modulus increases, indicating that most oscillation–amplitude of θ_2 comes from the worm shaft, not from worm tooth. On the other hand, the oscillation of θ_4 comes from the flexibility of worm-gear tooth. The effect the rigidity of worm-gear shaft is not important. The small reduction amplitude of θ_4 may be due to the deformation of worm helical tooth projects to the angle displacement direction of θ_4.

4.4. The effect of rigidity of worm and worm-gear teeth

Reference Fig. 6, as the spring constant of the gear teeth multiplied increases, the rigidity of worm and worm-gear teeth are also increase. As shown in Fig. 17, the maximum amplitude of θ_4 reduced very fast

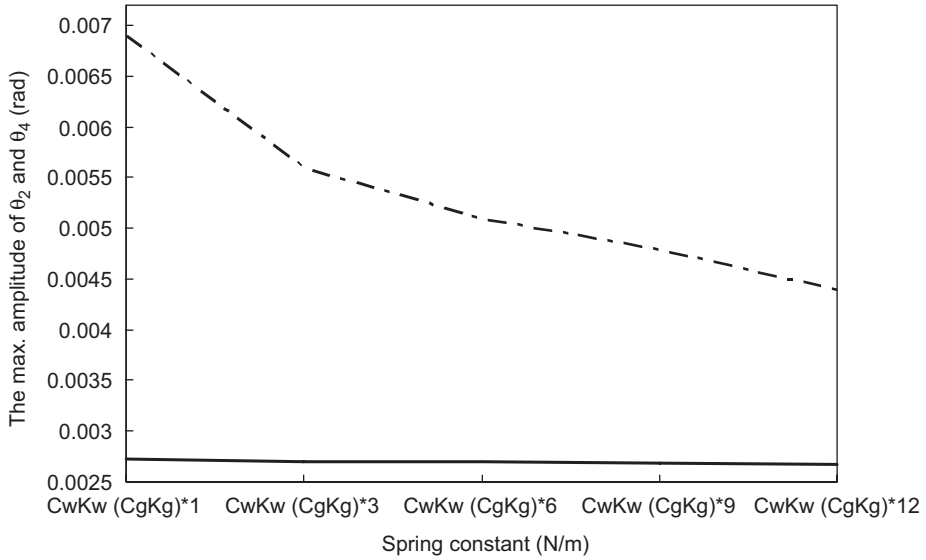

Fig. 17. The effect of teeth rigidity to the maximum oscillating amplitude of the worm and worm gear. —— θ_2, --- θ_4.

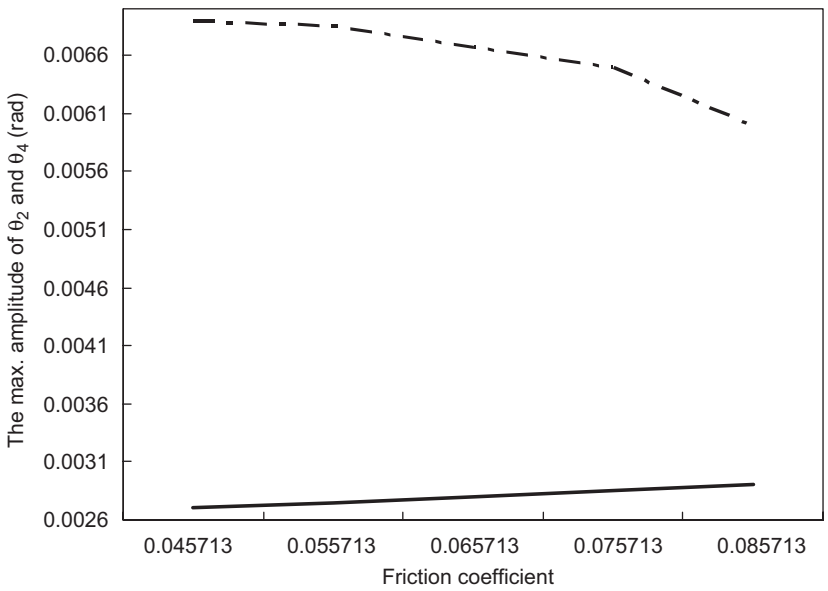

Fig. 18. The effect of friction coefficient to the maximum oscillating amplitude —— θ_2, --- θ_4.

compare with θ_2. This proves that the most important factor, which effects the oscillation of θ_4 is the rigidity of worm-gear tooth. The rigidity of the worm-gear shaft to the oscillation of θ_4 is not so important. Due to the lead angle of worm is small and the structure of worm tooth becomes very strong. It is also found that the most kinematics energy is stored in the worm-gear tooth, only small amount of the energy store in the worm. Therefore, the effect of the rigidity of the worm tooth is not as much as the effect of worm-gear tooth.

4.5. The friction

As shown in Fig. 18, when the friction is larger, the motor needs larger torque to conquer the friction force to keep up with the input angle in proportion to the angle acceleration of worm will increase. So when the motor is suddenly stopped, the rotation-inertia of worm and worm gear will increase a little. The friction force increases between worm tooth and worm-gear tooth and the amplitude of θ_4 decreases. The reason is evident in Eq. (15), while the lead angle (λ) of the worm is small, the effect of k_{3wg} is small.

5. Conclusions

In this study, the dynamic equilibrium equations of worm-gear set considering the rigidity of the tooth were developed. The analyzed results were compared with the measured data. The comparison shows that the mathematics model is reasonable correct. The influence of moment-inertia, friction, rigidity shaft and rigidity-gear tooth were also studied. The parameters study has following conclusions:

1. The diameter of the flywheel is reduced gradually, the amplitude of oscillating reduced gradually.
2. The larger the module of gear, the higher the maximum amplitude of angles θ_2 and θ_4.
3. Most oscillation of θ_2 comes from worm shaft, not from gear tooth. As to the oscillating of θ_4, the effect of the rigidity of the shaft is not important.
4. The effect of the rigidity of the gear tooth of the worm is not as much as that of worm gear.
5. The effect of friction is larger for θ_2 than that for θ_4.

Above conclusions indicate that when design a worm-gear set for high precision positioning, the rigidity of the worm gear is very important, that the material of the worm gear should be used more rigid material than that of the worm.

References

[1] C. Yuksel, A. Kahraman, Dynamic tooth loads of planetary gear sets having tooth profile wear, *Mechanism and Machine Theory* 39 (2004) 695–715.
[2] R.G. Parker, S.M. Vijayakar, T. Imajo, Non-linear dynamic response of a spur gear pair: modeling and experimental comparisons, *Journal of Sound and Vibration* 237 (3) (2000) 435–455.
[3] R. Maliha, U.C. Dogruer, H.N. Ozguven, Nonlinear dynamic modeling of gear-shaft-disk-bearing systems using finite elements and describing functions, *Journal of Mechanical Design* 126 (2004) 534–541.
[4] R.D. Britton, C.D. Elcoate, M.P. Alanou, H.P. Evans, R.W. Snidle, Effect of surface finish on gear tooth friction, *Journal of Tribology* 122 (2000) 354–360.
[5] S. Kong, K. Sharif, H.P. Evans, R.W. Snidle, Elastohydrodynamics of a worm gear contact, *Journal of Tribology* 123 (2001) 268–275.
[6] D.T. Tuttle, P.W. Seeing, A nonlinear model of a harmonic drive gear transmission, *IEEE Transactions on Robotics and Automation* 12 (3) (1996) 368–374.
[7] B.A. Helouvry, A survey of models, analysis tools and compensation methods for the control of machines with friction, *Automatica* 30 (7) (1994) 1083–1138.
[8] P. Doupont, Avoiding stick–slip in position and force control through feedback, *Proceedings of the 1991 IEEE International Conference on Robotics and Automation, Sacramento*, California, pp. 1470–1475.
[9] F. Oguri, C.-F. Chang, *Design Handbook of Charts and Standards for Mechanical Engineers*, eighth ed., Tai-Lung Book Co., Taiwan, 1982.
[10] J.E. Shigley, R.C. Mischke, *Mechanical Engineering Design*, fifth ed., McGraw-Hill, New York, 1989.
[11] V. Simon, Stress analysis in double enveloping worm gears by finite element method, *Journal of Mechanical Design* 115 (1994) 179–185.
[12] M. Octrue, A new method for designing worm gears, *Gear Technology: the Journal of Gear Manufacturing July/Aug* (1989) 30–35.

[13] K. Sudoh, Y. TanaKa, S. Matsumoto, Y. Tozaki, Load distribution analysis method for cylindrical worm gear teeth (measurement of deflection of worm gear teeth using laser holographic interferometer), *Japanese Mechanical Association* 59 (566) (1993) 265–271.
[14] Japan Gear Manufacturer Association Standard, JGMA301-01 Basic Contact Pattern of Gears and their inspection methods, 1971.
[15] B.W. Bair, C.B. Tsay, Characteristic Study on ZK-Type Dual-Lead Worm Gear Drives, thesis, Department of Mechanical Engineering, National Chiao Tung University, Taiwan, 1998.
[16] H.S. Fang, C.B. Tsay, Mathematical model and bearing contacts of the ZK-type worm gear set cut by oversize hob cutters, *Mechanism and Machine Theory* 31 (3) (1996) 271–282.
[17] I.H. Seol, The design, generation, and simulation of meshing of worm-gear drive with longitudinally localized contacts, *Journal of Mechanical Design* 122 (2000) 201–206.
[18] P.W. Crosher, *Design and Application of the Worm Gear*, first ed., ASME Press, New York, 2002.